Supplemental Information for:

Compartmentalized AMPK Signaling Illuminated by Genetically Encoded Molecular Sensors and Actuators

Authors:

Takafumi Miyamoto, Elmer Rho, Vedangi Sample, Hiroki Akano, Masaki Magari, Tasuku Ueno, Kirill Gorshkov, Melinda Chen, Hiroshi Tokumitsu, Jin Zhang, and Takanari Inoue

(1) Supplemental Figure S1-S7 and Supplemental Table S1 with legends

(1) Supplemental Figures

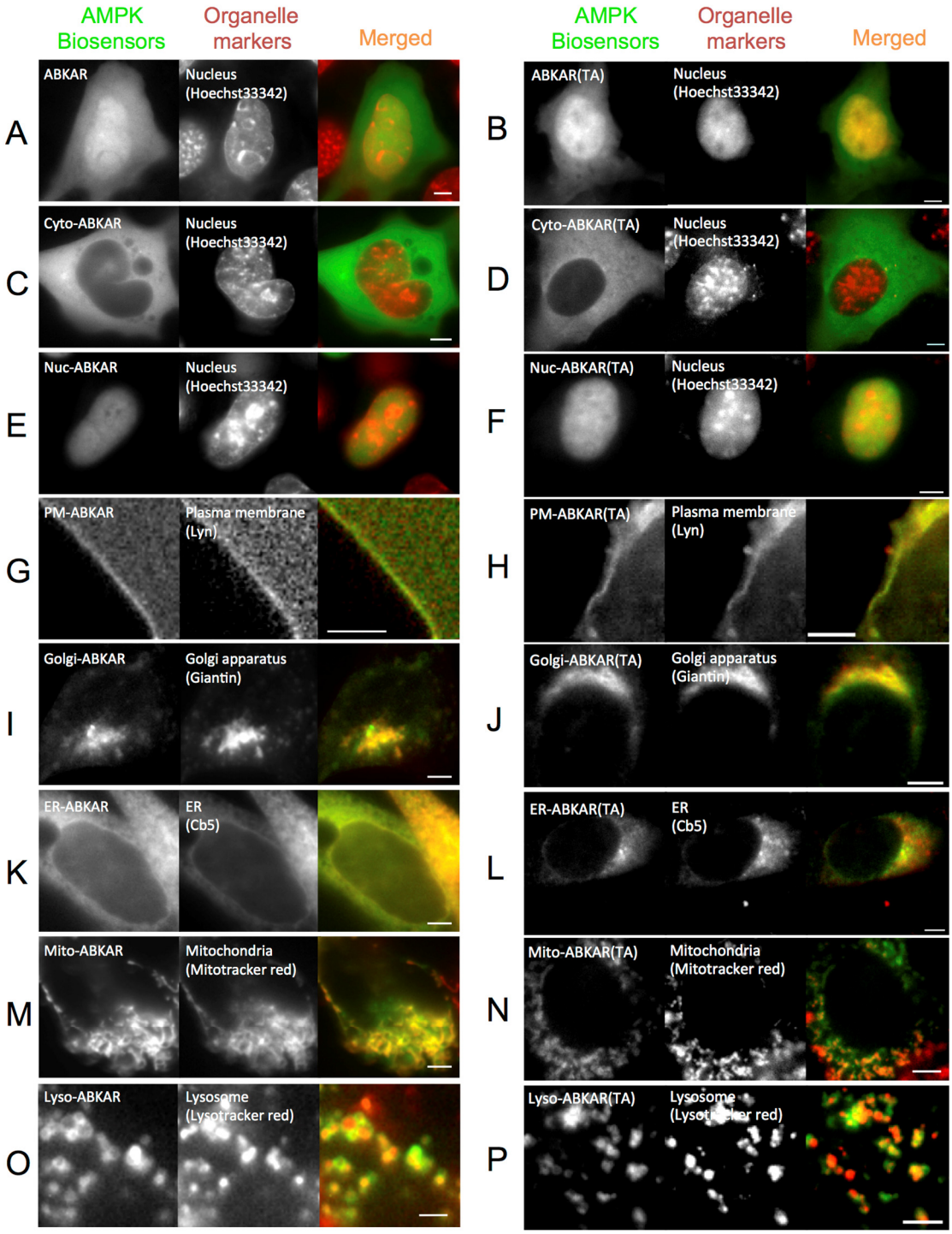

Supplemental Figure S1, Miyamoto et al.

Figure S1. Localization of ABKAR, osABKAR, and osABKAR (TA), Related to Figure 1.

(A) Left: Representative YFP image of ABKAR in WT MEFs. Middle: corresponding cells stained by Hoechst 33342. Right: Merged image.

(B) Left: Representative YFP image of ABKAR (TA) in WT MEFs. Middle: corresponding cells stained by Hoechst 33342. Right: Merged image.

(C) Left: Representative YFP image of Cyto-ABKAR in WT MEFs. Middle: corresponding cells stained by Hoechst 33342. Right: Merged image.

(D) Left: Representative YFP image of Cyto-ABKAR (TA) in WT MEFs. Middle: corresponding cells stained by Hoechst 33342. Right: Merged image.

(E) Left: Representative YFP image of Nuc-ABKAR in WT MEFs. Middle: corresponding cells stained by Hoechst 33342. Right: Merged image.

(F) Left: Representative YFP image of Nuc-ABKAR (TA) in WT MEFs. Middle: corresponding cells stained by Hoechst 33342. Right: Merged image.

(G) Left: Representative YFP image of PM-ABKAR in WT MEFs. Middle: corresponding cells expressing Lyn-mChF. Right: Merged image.

(H) Left: Representative YFP image of PM-ABKAR (TA) in WT MEFs. Middle: corresponding cells expressing Lyn-mChF. Right: Merged image.

(I) Left: Representative YFP image of Golgi-ABKAR in WT MEFs. Middle: corresponding cells expressing mChF-Giantin. Right: Merged image.

(J) Left: Representative YFP image of Golgi-ABKAR (TA) in WT MEFs. Middle: corresponding cells expressing mChF-Giantin. Right: Merged image.

(K) Left: Representative YFP image of ER-ABKAR in WT MEFs. Middle: corresponding cells expressing mChF-Cb5 Right: Merged image.

(L) Left: Representative YFP image of ER-ABKAR (TA) in WT MEFs. Middle: corresponding cells expressing mChF-Cb5 Right: Merged image.

(M) Left: Representative YFP image of Mito-ABKAR in WT MEFs. Middle: corresponding cells stained by Mitotracker red. Right: Merged image.

(N) Left: Representative YFP image of Mito-ABKAR (TA) in WT MEFs. Middle: corresponding cells stained by Mitotracker red. Right: Merged image.

(O) Left: Representative YFP image of Lyso-ABKAR in WT MEFs. Middle: corresponding cells stained by Lysotracker red. Right: Merged image.

(P) Left: Representative YFP image of Lyso-ABKAR (TA) in WT MEFs. Middle: corresponding cells stained by Lysotracker red. Right: Merged image.

Scale bars, 10 μm.

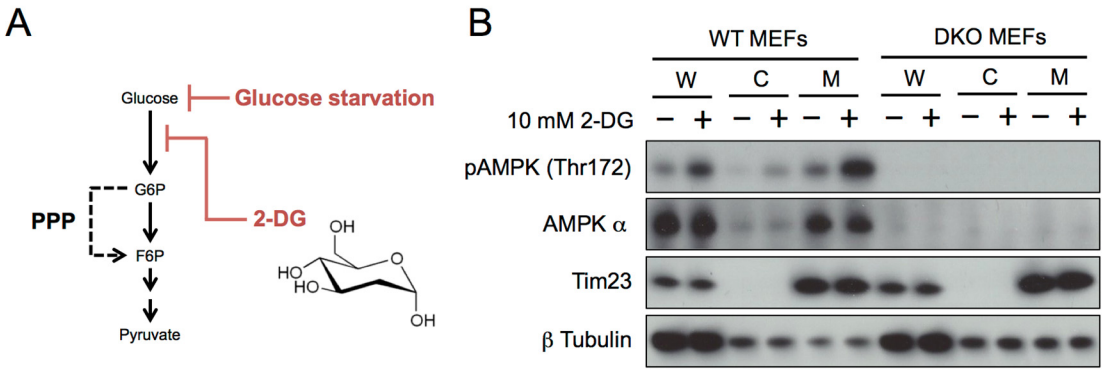

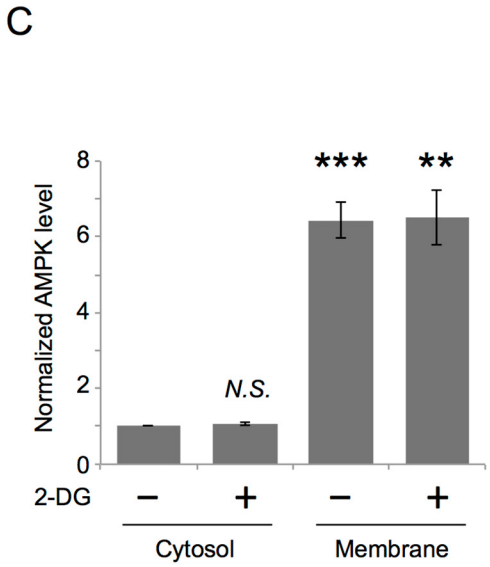

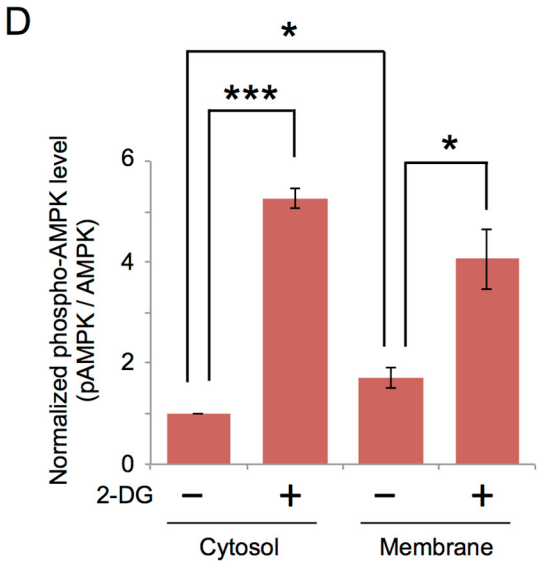

Supplemental Figure S2, Miyamoto et al.

Figure S2. Subcellular localization of AMPK, Related to Figure 1.

(A) Inhibitory mechanisms of two independent metabolic perturbation inputs.

(B) WT MEFs and DKO MEFs were treated with or without 10 mM 2-DG for 20 minutes. Subsequently these were subjected to the fractionation assay. W: whole cell lysate. C: cytosolic compartment. M: membrane compartment. Representative western blot image was shown.

(C) AMPK level in each cytosolic or membrane compartment in WT MEFs were determined by immunoblot analysis performed in Figure S2B. Quantification was performed on three independent experiments. Data are presented as mean ± standard error.

(D) Phosphorylated AMPK level in cytosolic or membrane compartment in WT MEFs were determined by immunoblot analysis performed in Figure S2B. Quantification was performed on three independent experiments. Data are presented as mean ± standard error.

*$p < 0.05$, **$p < 0.01$. ***$p < 0.001$. *N.S.,* statistically nonsignificant.

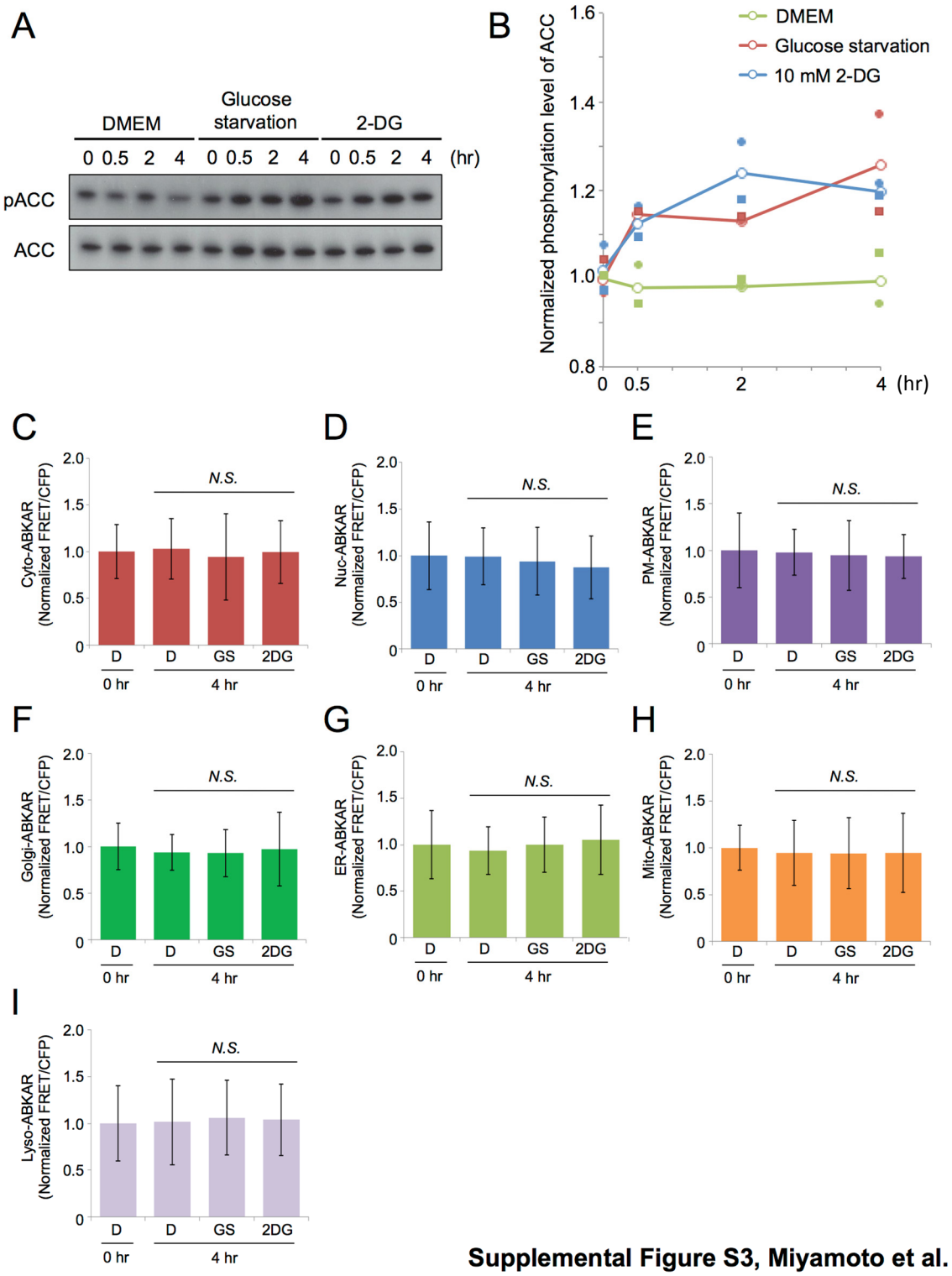

Supplemental Figure S3, Miyamoto et al.

Figure S3. AMPK activity in response to metabolic perturbation inputs, Related to Figure 2.

(A) WT MEFs were treated with indicated conditions and duration, and were subsequently subjected to western blot assay. Representative western blot is shown.

(B) Quantification of Figure S3A was performed on two independent experiments. Data are presented as mean.

(C-I) DKO MEFs were transiently transfected with indicated osABKAR, then AMPK activity was subsequently measured at each subcellular compartment under indicated condition. D: DMEM. GS: glucose starvation. 2DG: 10 mM 2-DG. Measured FRET/CFP ratio was normalized to the cells incubated with DMEM for 0 hour. Quantification was performed on three independent experiments. Data are presented as mean ± standard deviation. *N.S.,* statistically nonsignificant.

(C) AMPK activity in cytosol before (DMEM at 0 hour: n = 10) and after 4 hours (DMEM: n= 13, glucose starvation: n = 16, 2-DG: n = 15) in DKO MEFs as reported by Cyto-ABKAR.

(D) AMPK activity in nucleus before (DMEM at 0 hour: n = 19) and after 4 hours (DMEM: n= 19, glucose starvation: n = 18, 2-DG: n = 19) in DKO MEFs as reported by Nuc-ABKAR.

(E) AMPK activity at plasma membrane before (DMEM at 0 hour: n = 11) and after 4 hours (DMEM: n= 15, glucose starvation: n = 11, 2-DG: n = 13) in DKO MEFs as reported by PM-ABKAR.

(F) AMPK activity at Golgi apparatus before (DMEM at 0 hour: n = 12) and after 4 hours (DMEM: n= 17, glucose starvation: n = 17, 2-DG: n = 11) in DKO MEFs as reported by Golgi-ABKAR.

(G) AMPK activity at ER before (DMEM at 0 hour: n = 11) and after 4 hours (DMEM: n= 9, glucose starvation: n = 13, 2-DG: n = 14) in DKO MEFs as reported by ER-ABKAR.

(H) AMPK activity at mitochondria before (DMEM at 0 hour: n = 19) and after 4 hours (DMEM: n= 22, glucose starvation: n = 21, 2-DG: n = 14) in DKO MEFs as reported by Mito-ABKAR.

(I) AMPK activity at lysosome before (DMEM at 0 hour: n = 12) and after 4 hours (DMEM: n= 21, glucose starvation: n = 15, 2-DG: n = 16) in DKO MEFs as reported by Lyso-ABKAR.

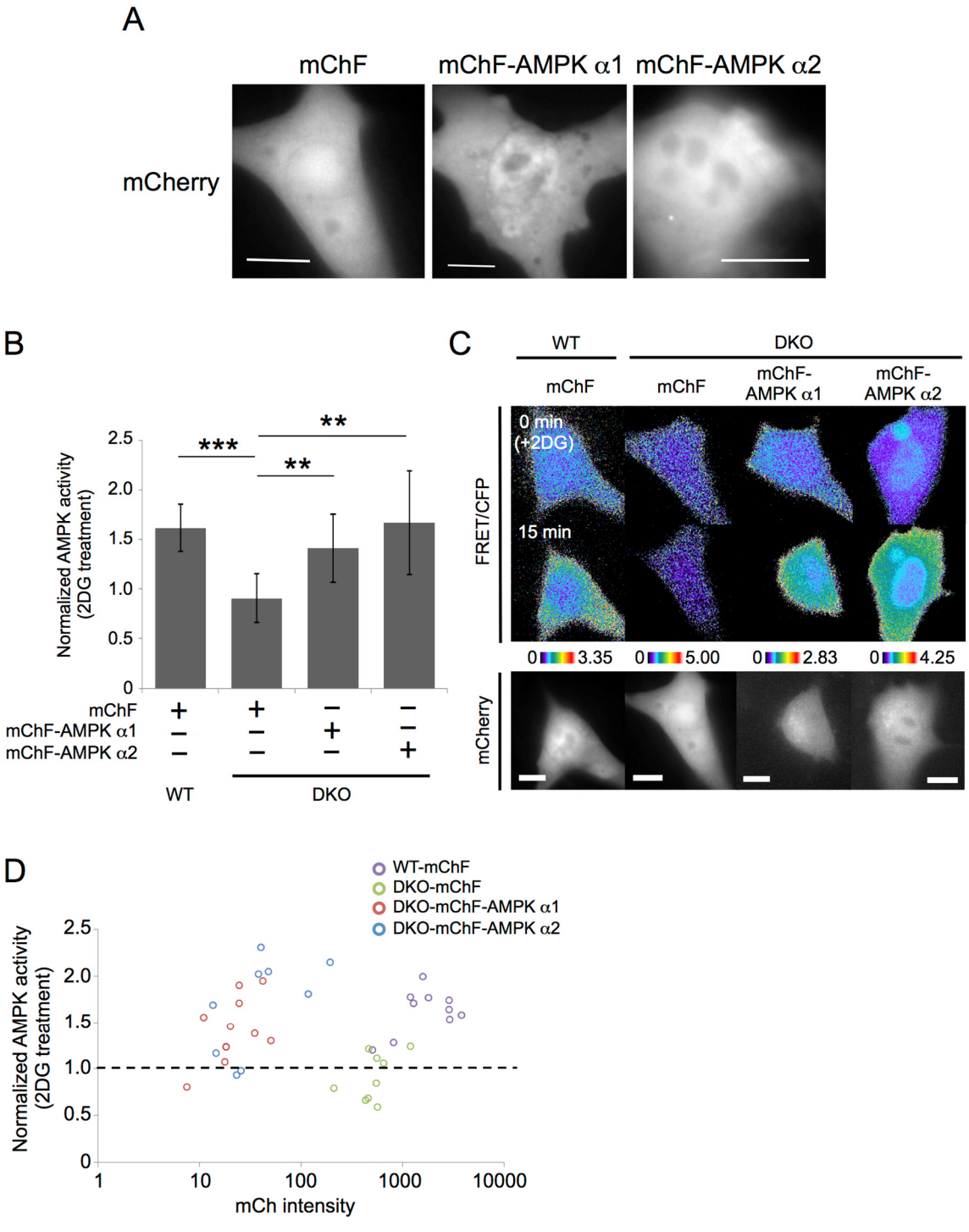

Supplemental Figure S4, Miyamoto et al.

Figure S4. Kinase activity of mChF-AMPK α1 and mChF-AMPK α2, Related to Figure 4.

(A) Localization of mChF, mChF-AMPK α1, and mChF-AMPK α2 in WT MEFs. Representative mCherry images are shown. Scale bar, 10 μm.

(B) AMPK activity in response to 2-DG stimulation. WT MEFs expressing mChF (n = 10), DKO MEFs expressing mChF (N = 9), DKO MEFs expressing mChF-AMPK α1 (N = 11), DKO MEFs expressing mChF-AMPK α2 (n = 9) were incubated with 10 mM 2-DG for 15 minutes. AMPK activity was monitored by ABKAR every 0.5 minute. Quantification was performed on three independent experiments. Data are presented as mean of normalized FRET/CFP ratio for last 2.5 minutes, ± standard deviation. **$p < 0.01$. ***$p < 0.001$.

(C) Representative FRET/CFP image in Figure S4B are shown.

(D) All analyzed data in Figure S4B is plotted.

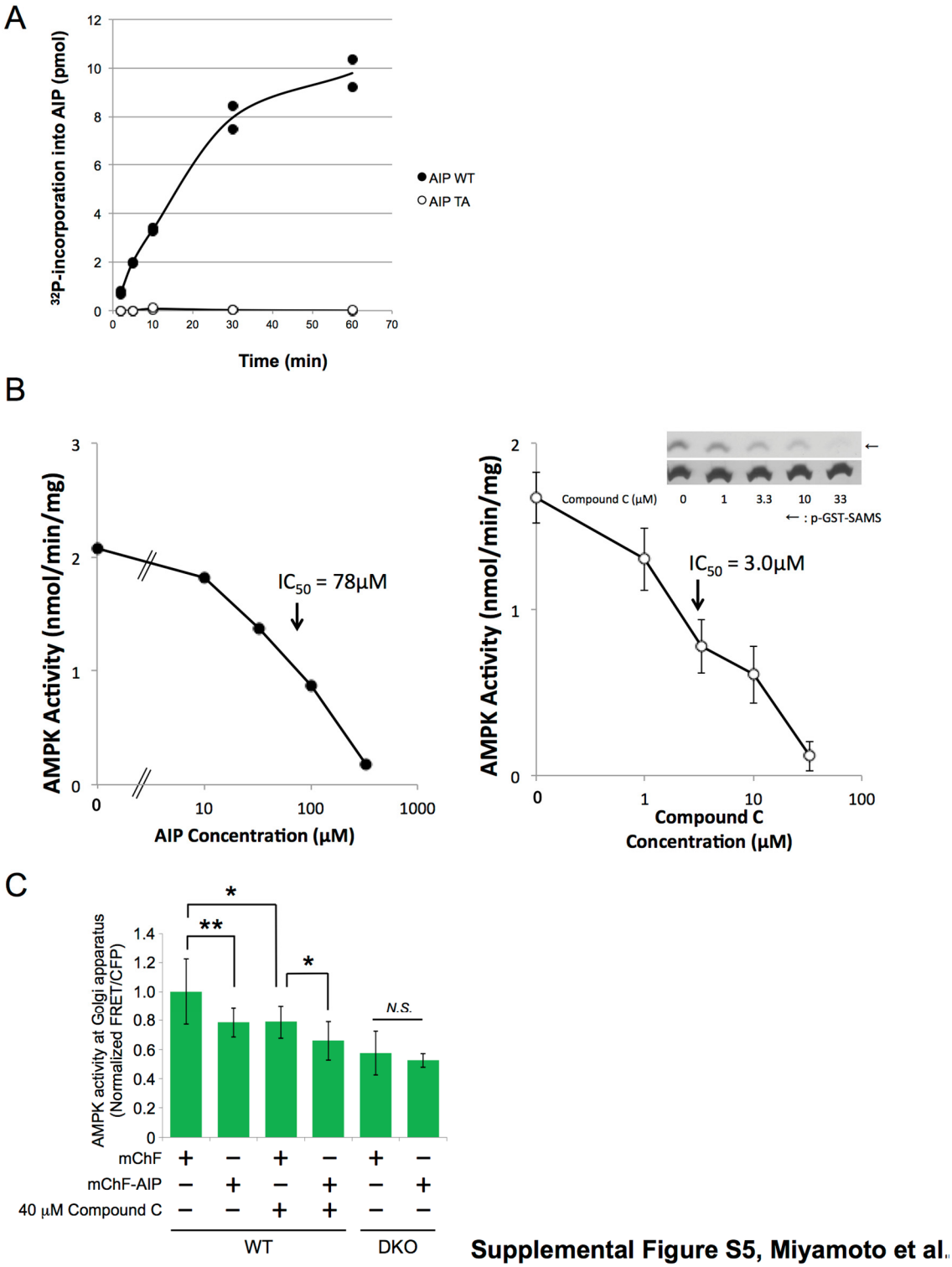

Supplemental Figure S5, Miyamoto et al.

Figure S5. Phosphorylation of AIP by activated AMPK and inhibition of AMPK activity by Compound C, Related to Figure 5.

(A) Activated AMPK and either 20 μM AIP or AIP (TA) was incubated with [γ-^{32}P]ATP. Subsequent ^{32}P incorporation into each AIP was measured at each time point. Quantification was performed on two independent experiments. Data are presented as mean.

(B) Activated AMPK was incubated with GST-SAMS and [γ-^{32}P]ATP in the presence of various concentrations of either AIP (left panel) or Compound C (right panel). ^{32}P incorporation into GST-SAMS was measured. Data of the inhibitory effect of Compound C (right panel) are presented as mean ± standard deviation. Quantification was performed on three independent experiments. Inset images indicate representative autoradiography (upper panel) and Coomassie Brilliant Blue staining (lower panel) of phosphorylated GST-SAMS.

(C) Inhibitory effect of AIP was compared with that of Compound C in living cells. WT MEFs or DKO MEFs were transiently transfected with indicated constructs and treated with or without Compound C. Subsequently, AMPK activity at Golgi apparatus in WT MEFs expressing mChF (Compound C (-): n = 25, (+): n = 9) or mChF-AIP (Compound C (-): n = 11, (+): n = 8) or in DKO MEFs expressing mChF (n = 13) or mChF-AIP (n = 11) was measured by Golgi-ABKAR. Quantification was performed on three independent experiments. Data are presented as mean ± standard deviation. *$p < 0.05$, **$p < 0.01$. *N.S.,* statistically nonsignificant.

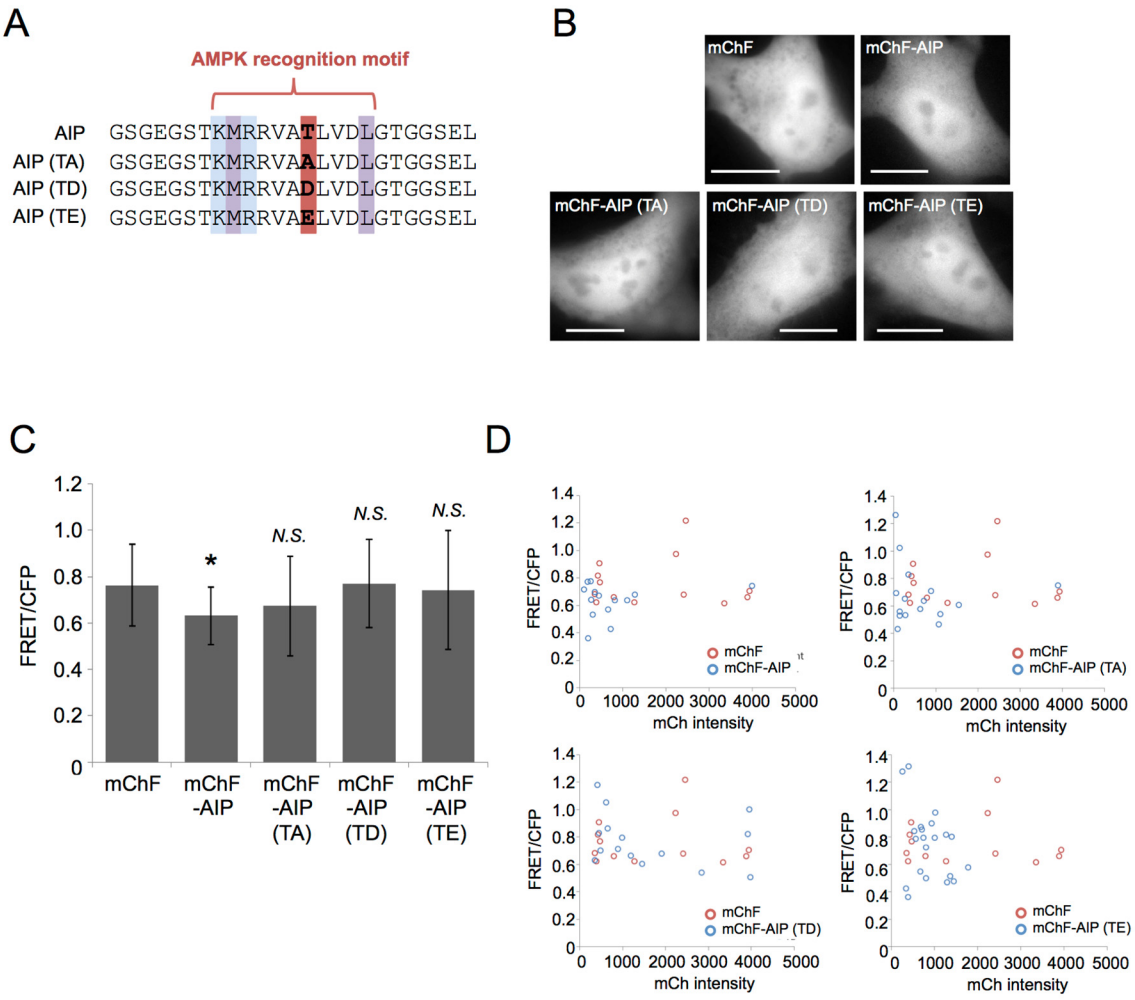

Supplemental Figure S6, Miyamoto et al.

Figure S6. The effect of phospho-mimic AIP on ABKAR, Related to Figure 5.

(A) Amino acid sequence alignment of AIP, AIP (TA), AIP (TD), and AIP (TE).

(B) Localization of mChF-AIP, mChF-AIP (TA), mChF-AIP (TD), and mChF-AIP (TE) in WT MEFs. Representative mCherry images are shown. Scale bar, 10 μm.

(C) AMPK activity in WT MEFs expressing ABKAR and either mChF (n = 13), mChF-AIP (n = 14), mChF-AIP (TA) (n = 16), mChF-AIP (TD) (n = 15), and mChF-AIP (TE) (n = 21) were measured from tree independent experiments. Data are presented as mean ± standard deviation. *$p < 0.05$. *N.S.,* statistically nonsignificant.

(D) All analyzed data in Figure S6C are plotted.

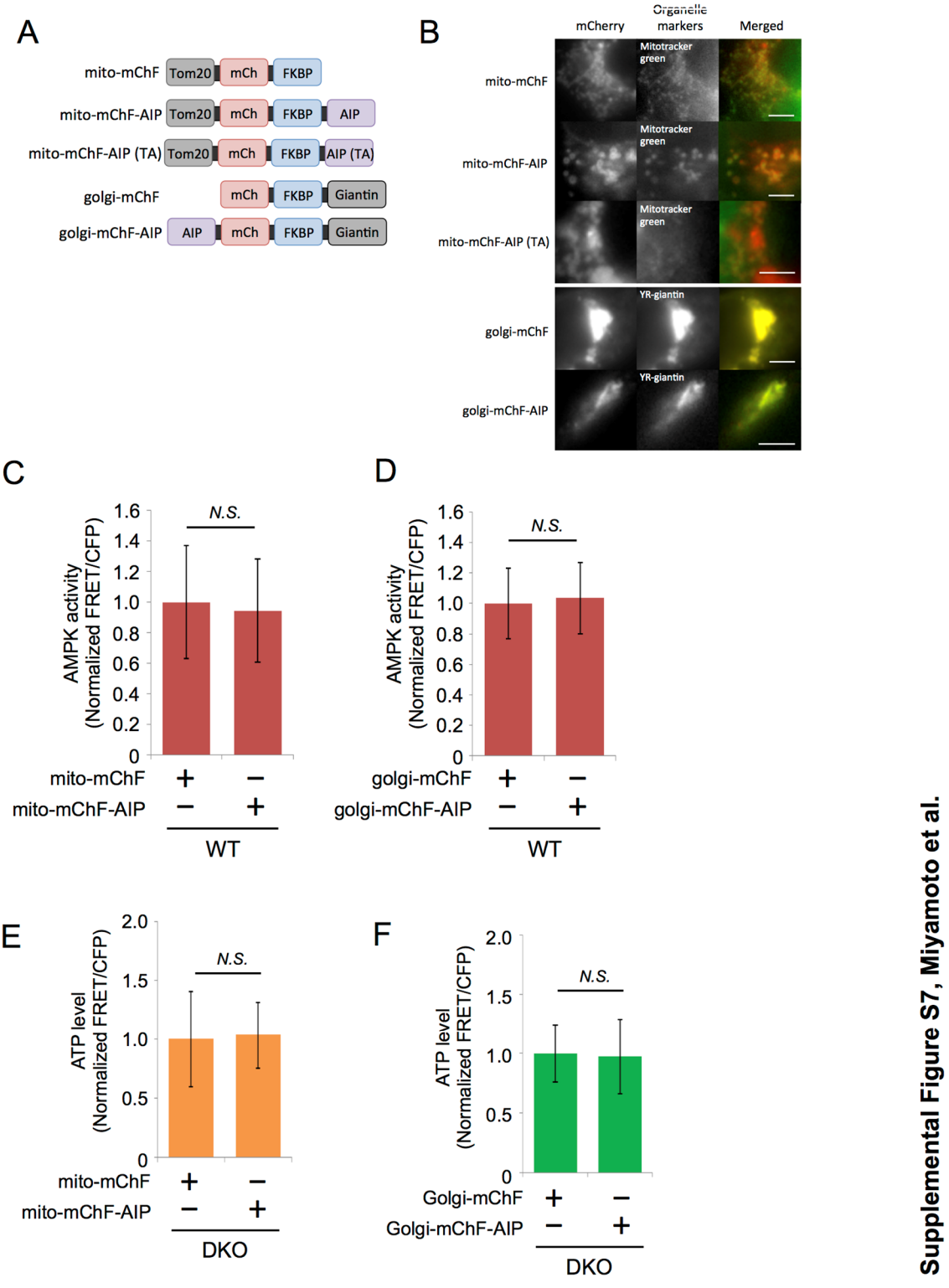

Supplemental Figure S7, Miyamoto et al.

Figure S7. Development of mitochondria and Golgi apparatus-specific AIP, Related to Figure 6.

(A) Schematic diagram of mito-mChF, mito-mCh-AIP, mito-mChF-AIP (TA), golgi-mChF, and golgi-mChF-AIP were shown. Tom20 is a targeting sequence for mitochondria. Giantin is a targeting sequence for Golgi apparatus.

(B) Localization of each construct in WT MEFs. Left: Representative mCherry image. Middle: corresponding organelle markers. Right: Merged image. Scale bar, 10 μm.

(C) AMPK activity in cytosolic compartment was measured by ABKAR in WT MEFs expressing either mito-mChF (n = 37) or mito-mChF-AIP (n = 40). Quantification was performed on three independent experiments. Data are presented as mean ± standard deviation. *N.S.,* statistically nonsignificant.

(D) AMPK activity in cytosolic compartment was measured by ABKAR in WT MEFs expressing either golgi-mChF (n = 49) or golgi-mChF-AIP (n = 49). Quantification was performed on three independent experiments. Data are presented as mean ± standard deviation. *N.S.,* statistically nonsignificant.

(E) Intracellular ATP level was measured by ATP biosensor in DKO MEFs expressing either mito-mChF (n = 40) or mito-mChF-AIP (n = 54). Quantification was performed on three independent experiments. Data are presented as mean ± standard deviation. *N.S.,* statistically nonsignificant.

(F) Intracellular ATP level was measured by ATP biosensor in DKO MEFs expressing either golgi-mChF (n = 57) or golgi-mChF-AIP (n = 49). Quantification was performed on three independent experiments. Data are presented as mean ± standard deviation. *N.S.,* statistically nonsignificant.

Name	Localization	OTS Position	Origin	NCBI Accession Number	Fused amino acid sequence
Cyto-ABKAR	Cytosol	C-terminus	HIV1-Rev	AGO06240.1	LPPLERLTL
Nuc-ABKAR	Nucleus	C-terminus	The SV40 large T-antigen	CBL95275	PKKKRKVED
PM-ABKAR	Plasma membrane	N-terminus	Tyrosine-protein kinase Lyn	XP_004313862	MGCIKSKRKDNLKD
Golgi-ABKAR	Golgi apparatus	N-terminus	Nitric oxide synthase, endothelial	XP_004702531.1	MGNLKSVAQEPGPPCGLGLGL GLGLCGKQGPA
ER-ABKAR	Endoplasmic reticulum	N-terminus	Cytochrome P450 2C1	AAA31436	MDPVVVLGLCLSCLLLLSLWK QSYGGG
Mito-ABKAR	Mitochondria	N-terminus	A kinase anchor protein 1	AAC27100	MAIQLRSLFPLALPGMLALLGW WWFFSRKKA
Lyso-ABKAR	Lysosome	N-terminus	LAMP1	NP_005552	MAAPGSARRPLLLLLLLLLLGL MHCASAAMFMVKNGNGTACI MANFSAAFSVNYDTKSGPKN MTFDLPSDATVVLNRSSCGKE NTSDPSLVIAFGRGHTLTLNFT RNATRYSVQLMSFAYNLSDTH LFPNASSKEIKTVESITDIRADID KKYRCVSGTQVHMNNVTVTP HDATIQAYLSNSSFSRGETRCE QDRPSPTTAPPAPPSPSPSPV PKSPSVDKYNVSGTNGTCLLA SMGLQLNLTYERKDNTTVTRL LNINPNKTSASGSCGAHLVTLE LHSEGTTVLLFQFGMNASSSR FFLQGIQLNTILPDARDPAFKAA NGSLRALQATVGNSYKCNAEE HVRVTKAFSVNIFKVWVQAFK VEGGQFGSVEECLLDENSMLI PIAVGGALAGLVLIVLIAYLVGRK RSHAGYQTI

Supplemental Table S1, Miyamoto et al.

Table S1. Targeting sequence of osABKAR, Related to Figure 1.

Organelle-targeting sequences used in each osABKAR are listed. Same organelle-targeting sequence was used for corresponding osABKAR (TA).

(2) Supplemental Text

To further characterize the correlation of the osABKAR FRET signal with different AMPK activity states, we measured the FRET signal in each compartment in WT MEFs that expressed either a dominant negative form of the AMPK α1 subunit (K45R mutant, Dyck et al., 1996, known as AMPK-DN) or a constitutively active form of AMPK α subunit (aa1-312, Kimura et al., 2003, known as AMPK-CA), referred to as AMPK-DN cells and AMPK-CA cells, respectively. To label AMPK-CA and AMPK-DN, we fused the mCherry-FK506 binding protein conjugated protein (mChF) to the N-terminus of each of the constructs. Similar to mChF, both mChF-AMPK-DN and mChF-AMPK-CA were localized uniformly in cells. As expected, mChF-AMPK-DN reduced the FRET signal in cytosol, but not in the nucleus as reported by ABKAR. To further examine the effect of AMPK-DN at each subcellular location, we expressed osABKAR in WT MEFs. As a result, the expression of mChF-AMPK-DN reduced the FRET signal in the cytosol by 15.3 ± 4.8% (Cyto-ABKAR: n = 45 in control cells; n = 56 in AMPK-DN cells), by 16.0 ± 3.2% at the plasma membrane (PM-ABKAR: n = 57 in control cells; n = 50 in AMPK-DN cells), by 27.1 ± 2.8% at the Golgi apparatus (Golgi-ABKAR: n = 53 in control cells; n = 37 in AMPK-DN cells), by 24.9 ± 3.2% at the ER (ER-ABKAR: n = 54 in control cells; n = 63 in AMPK-DN cells), by 18.4 ± 3.0% at the mitochondria (Mito-ABKAR: n = 50 in control cells; n = 49 in AMPK-DN cells), and by 21.5 ± 5.5% at the lysosome (Lyso-ABKAR: n = 42 in control cells; n = 22 in AMPK-DN cells). The FRET signal in the nuclear compartment was not affected by mChF-AMPK-DN expression based on Nuc-ABKAR (−4.7 ± 4.2%; n = 56 in control cells; n = 49 in AMPK-DN cells). Furthermore, mChF-AMPK-CA expression resulted in an increase of over 50% in the FRET signal in the cytosolic and nuclear compartments (Cyto-ABKAR: 76.2 ± 6.6%; n = 36 in control cells; n = 35 in AMPK-CA cells, Nuc-ABKAR: 52.3 ± 9.7%; n = 32 in control cells; n = 34 in AMPK-CA cells) as well as in cells that expressed diffusive ABKAR (cytosolic region: 115.5 ± 9.0%; nuclear region: 76.2 ± 7.4%; n = 32 in control cells; n = 34 in AMPK-CA cells). In contrast, mChF-AMPK-CA caused a modest increase of approximately 30% in the FRET signal of membrane compartments (plasma membrane: 24.9 ± 5.8%; n = 20 in control cells; n = 27 in AMPK-CA cells, Golgi apparatus: 29.0 ± 6.7%; n = 32 in control cells; n = 33 in AMPK-CA cells, ER: 39.4 ± 5.5%; n = 23 in control cells; n = 25 in AMPK-CA cells, mitochondria: 26.4 ± 5.1%; n = 45 in control cells; n = 56 in AMPK-CA cells, lysosome: 25.5 ± 3.4%; n = 38 in control cells; n = 44 in AMPK-CA cells) where the basal FRET signal was relatively higher than those in other compartments. In general, there is little to no correlation between the observed ABKAR signals and the protein expression level we tested ($-0.42 < r < 0.35$), except one case where the Nuc-ABKAR signal positively correlated with mChF-AMPK-CA expression ($r = 0.76$). Figures corresponding to these data cannot be incorporated in the supplemental information due to a limited space.

(3) Supplemental Experimental Procedures

Materials

Anti-phospho-AMPK (Thr172), anti-AMPK, anti-phospho-ACC and anti-ACC antibodies were purchased from Cell Signaling Technology. Anti-β Tubulin antibody was purchased from Abcam. Anti-Tim23 antibody was purchased from BD Transduction Laboratories. 2-DG and Compound C were purchased from Sigma and EMD Millipore, respectively. Mitotracker red and Mitotracker green were purchased from Invitrogen. Plasmid encoding ATP biosensor was kindly provided by Dr. Hiromi Imamura (Kyoto University). Recombinant AMPK was expressed in *E.coli* BL21 (DE3) by using the tricistronic plasmid pγ1β1His-α1 (kindly provided by Dr. Dietbert Neumman, Swiss Federal Institute of Technology, Zurich, Switzerland) followed by purification with Ni-NTA agarose chromatography (Qiagen) (Neumann et al., 2003). Expression and purification of GST-SAMS (GST-SAMS expression plasmid was kindly provided by Dr. Hiroyasu Esumi, Tokyo University of Science, Chiba, Japan) was carried out by the method of Kishimoto *et al.* (Kishimoto et al., 2006).

Plasmid Construction

For NES and NLS targeting, ABKAR was subcloned into pcDNA3 vector containing the sequence coding for 5'- LPPLERLTL and 5'- PKKKRKVED at the C terminus between EcoRI and XbaI sites, respectively. To create NES and NLS targeting ABKAR(TA), ABKAR(TA) was subcloned into NES and NLS targeting ABKARs using Kpn1 and BamH1 to replace ABKAR. For plasma membrane, Golgi apparatus, ER, mitochondria and lysosome targeting, ABKAR was subcloned into pcDNA3 vector containing the sequence coding 14 amino acids from tyrosine protein kinase Lyn, 32 amino acids from eNOS, 27 amino acids from cytochrome p450, 31 amino acids from A kinase anchor protein, 417 amino acids from LAMP1 at the N terminus between HindIII and BamHI sites, respectively. In addition, ABKAR(TA) was subcloned into each organelle targeting ABKAR constructs using BamH1 and EcoR1 to replace ABKAR but to create Lyso-ABKAR(TA), HindIII and BamH1 were used to subclone lysosome targeting sequences into ABKAR(TA) vector at the N terminus. The pH probe was created by using EcoR1 and BamH1 to subclone Venus(H148G) into the CFP vector.

Plasmid coding wild-type AMPK α1 subunit, α2 subunit, constitutively active form of AMPK (amino acid 1-312), and dominant negative form of AMPK α 1 were kindly provided by Dr. Gabriele Ronnett (Johns Hopkins University). These AMPK genes were subcloned into the mCherry-FKBP (mChF) vector between EcoRI and BamHI sites. For genetically encoded AMPK inhibitor peptide, GSGEGSTKMRRVATLVDLGTGGSEL (termed mChF-AIP), GSGEGSTKMRRVAALVDLGTGGSEL (termed mChF-AIP (TA)), GSGEGSTKMRRVADLVDLGTGGSEL (termed mChF-AIP (TD)), and GSGEGSTKMRRVAELVDLGTGGSEL (termed mChF-AIP (TE)) were subcloned into the mChF vector between EcoRI and BamHI sites. For mitochondria-specific mChF, mChF-AIP, and mChF-AIP (TA), mitochondria-targeting sequence described previously

(Komatsu et al., 2010) was inserted at the N-terminus of each construct (termed mito-mChF, mito-mChF-AIP, and mito-mChF-AIP (TA), respectively). To anchor mChF at Golgi apparatus, Golgi-apparatus-targeting sequence described previously (Komatsu et al., 2010) was inserted into the C-terminus of mChF (termed Golgi-mChF). For Golgi-apparatus-specific AIP, AIP-coding sequence was subcloned at N-terminus of Golgi-mChF.

Cell culture and transfection

WT MEFs, DKO MEFs, HEK293, and Cos7 cells were cultured in Dulbecco's modified Eagle's medium (DMEM; Gibco) supplemented with 10% fetal bovine serum and 1% penicillin/streptomycin at 37°C in 5% CO_2. For all transient transfection, cells were transfected with the respective DNA constructs by plating them directly in a transfection solution containing DNA plasmid and FuGENE HD (Roche). Cells were plated on poly-D-Lysine hydrobromide (Sigma)-coated cover glass, and then cultured in 6-well plates. Both imaging and western blot analysis was carried out 36 to 48 hours after transfection. For glucose starvation, cells were cultured in glucose withdrawal medium (Gibco).

Live-cell Imaging

CFP, YFP, and mCherry excitation were carried out by an X-Cite Series 120Q mercury vapor lamp and processed through appropriate filter cubes. Images were taken using a 63× objective (Plan-Apochromat, NA=1.4, Zeiss) mounted on an inverted Axiovert 135 TV microscope (Zeiss) and were captured by a QIClick charge-coupled device camera (QImaging). Imaging was driven by Metamorph 7.5 imaging software (Molecular Devices). All imaging experiments were completed at room temperature (21-23°C). FRET images were thresholded to remove background before any contrast adjustments. To measure a FRET value over CFP intensity (referred to as FRET/CFP), we chose three independent regions in each organelle based on the YFP images, and then FRET and CFP intensity values in the corresponding region was automatically calculated by Metamorph 7.5 imaging software. The average of FRET/CFP was calculated from at least three independent experiments. Cells with abnormal organelle morphology, for example disassembled Golgi apparatus, were excluded from analysis.

Measurement of intracellular pH level

For intracellular pH measurement before and after metabolically perturbed condition, WT MEFs expressing pH biosensor were incubated in either DMEM containing glucose, glucose-starved DMEM, or DMEM containing 10 mM 2-DG for thirty minutes.

For intracellular pH measurement in real-time, WT MEFs expressing the pH biosensor were imaged with phenol red-free DMEM with glucose. 10 mM 2-DG was added to the dish at time 0. The pH 5.2 buffer and two proton ionophores nigericin and monensin were used at 5 μM concentrations to decrease the pH of

the cells as a positive control. Cells were imaged in 1 mL of media on an Axiovert 200M epifluorescence microscope with a 40x/1.3 NA oil-immersion objective lens and a cooled charge-coupled device camera (Roper Scientific, Trenon, NJ) controlled by Metafluor 7.7 software (Molecular Devices, Sunnyvale, CA). Dual cyan/yellow emission ratio imaging was performed using a 420DF20 excitation filter, a 450 DRLP dichroic mirror, and two emission filters (475DF40 for CFP and 535DF25 for YFP). Filter sets were alternated using a Lambda 10-2 filter changer (Sutter Instruments, Novato, CA). Images were taken every 1 minute. Raw fluorescence images were corrected by subtracting the background fluorescence intensity of a cell-free region from the emission intensities of biosensor expressing cells. Yellow/cyan intensity ratios were then calculated at each time point. All time courses were normalized by dividing the intensity ratio at each time point by the basal value immediately preceding drug addition.

Western Blotting

Total cell lysates were prepared with lysis buffer containing 50 mM Tris-HCl (pH 7.5), 100 mM NaCl, 1% NP-40, protease inhibitor cocktail (Roche), and phosphatase inhibitor cocktail (Sigma) and normalized by protein concentration using BCA method (Thermo Scientific). Cytosolic and membrane fraction sample were prepared using FOCUS SubCell kit (G-BIOSCIENCES). For western blotting, protein samples were separated on 4%-20% SDS-PAGE and transferred to PVDF membrane (GE Healthcare). Membranes were blocked in PBS containing 10% nonfat milk for 1 hour at room temperature. Then the membranes were incubated with primary antibodies according to the manufacturer's instruction for 18 hours at 4°C. The membranes were subsequently incubated with horseradish peroxidase-conjugated goat anti-rabbit or anti-mouse IgG (Cell Signaling) for enhanced chemiluminescence detection (Thermo Scientific). Image quantification was performed by Image J (NIH) from two to three independent experiments.

Peptide synthesis

Peptides were synthesized by standard Fmoc/*t*Bu strategy using HATU/DIPEA for coupling and 40% piperidine (40%) in DMF for Fmoc deprotection as described before (Ref: Chemistry - A European Journal 17, 14763–14771, 2011). Automated peptide syntheses were performed on Syro I Parallel Peptide Synthesis System: fully automated computer controlled peptide synthesizer equipped with a one arm pipetting robot and 24 x 5 mL reactor block (S1PS-3B, Biotage). The reactions were performed in a peptide vessel comprising a sintered glass filter and a 3-way stopcock (GL-25, CHEMGLASS).

Briefly, chlorotrityl chloride resin (100-200 mesh, 1% DVB substitution, 30 mg, 1.33 mmole,g^{-1}) was placed in a reaction vessel. The resin is preswollen in DMF for 1 h and then filtered off. First amino acid was attached to the resin and then Fmoc was deprotected. Subsequently, Fmoc-protected amino acids were sequentially coupled to the resin-bound amino acid from the carboxyl to amino terminus. At the end of reaction, the resin was washed with dichloromethane several times and dried *in vacuo*. Peptide cleavage

from the resin and concomitant removal of the amino acid side-chain protecting groups were accomplished by shaking with TFA/triethylsilane/H_2O (98:1:1 v/v/v) for 2h at ambient temperature. The resin was filtrated and washed twice with CH_3CN/H_2O containing 0.1% TFA (v/v). The filtrate was concentrated *in vacuo* and purified by RP-HPLC equipped with PDA detector (Jasco PU-2080 system); column: Inertsil OSD-3 Octadecyl Prep Column (ϕ:5 μm, 10 x 250 mm, 5020-06812, GL Sciences); eluent: eluent A (H_2O containing 0.1% TFA (v/v)) and eluent B (CH_3CN with 20% H_2O containing 0.1% TFA (v/v)), a 20-min linear gradient from 5% to 100% solvent B; flow rate, 5.0 mL/min; detection wavelength, 210 nm. Freeze-drying of HPLC fractions gave off-white powders. Synthesized peptides were characterized by MALDI-TOF mass spectrometry (AXIMA-TOF^2 spectrometer, Shimadzu); AIP: *m/z* 2478 $[M+H]^+$, AIP(TA) *m/z* 2449 $[M+H]^+$.

***In vitro* AMPK activity assay**

Recombinant AMPK (20 ng) maximally activated by phosphorylation with Ca^{2+}/calmodulin-dependent protein kinase kinase β (CaMKKβ), was incubated with 10 μg of purified GST-SAMS (substrate) and 100 μM [γ-^{32}P]ATP in a solution (20 μl) containing 50 mM HEPES (pH 7.5), 10 mM $Mg(Ac)_2$, 1 mM DTT and 1 mM EGTA at 30 ^oC for 30 min in the presence of various concentrations of either AIP or AIP (TA) (0–330 μM in Me_2SO at a final concentration of 10%) or Compound C (0-33 μM in Me_2SO at a final concentration of 10%). A 30-min reaction was chosen to determine AMPK activity based on the time course experiment (data not shown). After termination of the reaction by addition of 2 x SDS-PAGE sample buffer (5 μl), samples (20 μl) were subjected to SDS-12.5% PAGE followed by autoradiography (Figure 5B) and then ^{32}P-incorporation into GST-SAMSs were determined by Cerenkov counting of excised gels (Figure 5C).

(4) Supplemental References

Dyck, J.R.B., Gao, G., Widmer, J., Stapleton, D., Fernandez, C.S., Kemp, B.E., and Witters, L.A. (1996). Regulation of 5'-AMP-activated Protein Kinase Activity by the Noncatalytic and Subunits. J. Biol. Chem. *271*, 17798–17803.

Kimura, N., Tokunaga, C., Dalal, S., Richardson, C., Yoshino, K., Hara, K., Kemp, B.E., Witters, L. a, Mimura, O., and Yonezawa, K. (2003). A possible linkage between AMP-activated protein kinase (AMPK) and mammalian target of rapamycin (mTOR) signalling pathway. Genes Cells *8*, 65–79.

Kishimoto, A., Ogura, T., and Esumi, H. (2006). A pull-down assay for 5' AMP-activated protein kinase activity using the GST-fused protein. Mol. Biotechnol. *32*, 17–21.

Komatsu, T., Kukelyansky, I., McCaffery, J.M., Ueno, T., Varela, L.C., and Inoue, T. (2010). Organelle-specific, rapid induction of molecular activities and membrane tethering. Nat. Methods *7*, 206–208.

Neumann, D., Woods, A., Carling, D., Wallimann, T., and Schlattner, U. (2003). Mammalian AMP-activated protein kinase : functional , heterotrimeric complexes by co-expression of subunits in Escherichia coli. Protein Expr. Purif. *30*, 230–237.